Fabrication of Broadband MEMS Antennas and Application to Target Detection

Douglas A. Hutchings*[(1)] and Magda El-Shenawee [(2)]
(1) Microelectronics-Photonics Program
(2) Electrical Engineering Department
University of Arkansas, Fayetteville, AR. 727201
E-mail: dwoten@uark.edu

Introduction

This work details the fabrication processes for a broadband antenna on a MEMS steerable platform. The platform is capable of rotation around two independent axes through the use of four silicon torsion hinges similar to that reported in [1]-[2]. The device is fabricated using traditional bulk micromachining techniques. Silicon is used as the substrate material due to its well understood processing characteristics. The antenna is modified from the Fourpoint antenna [3] and operates between 10-16 GHz. The device is characterized using an HP 8510C Vector Network Analyzer and is used for target detection in a custom built anechoic chamber. An artificial neural network post processing algorithm is implemented on the measured data for the detection of metal, glass and wood spheres with a diameter of 3/8″.

Device Fabrication

A 300µm thick silicon wafer with a double sided polish is used as the base substrate. The fabrication consists of four major processing steps outlined in Fig. 1. The first step is using the Deep Reactive Ion Etching (DRIE) technique to create vias through the wafer to allow alignment of features on both sides of the wafer as shown in Fig. 1a. The through vias are necessary because a double sided alignment tool was not available. Once the vias are etched, a large cavity is etched in the backside of the wafer using wet etching to define a diaphragm that will become the free standing MEMS platform as shown in Fig. 1b. The antenna is defined on the topside of the diaphragm and then the DRIE process is used to free the MEMS platform as shown in Fig. 1. c and d respectively.

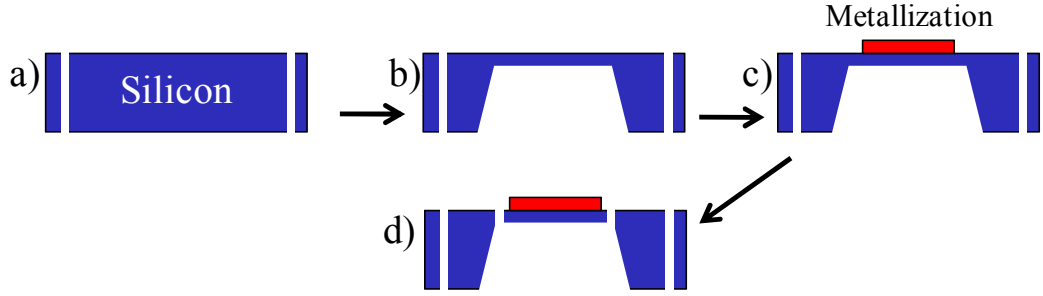

Fig. 1. Processing flowchart showing a) through-silicon vias b) backside cavity etch c) antenna metallization and d) platform release

Commercially available edge-mount SMA connectors are adhered to the antenna using H20E silver filled epoxy. The epoxy is cured in an annealing oven for an hour at 100ºC. The cured epoxy makes a strong conductive bond between the SMA connector and the

978-1-4244-4968-2/10/$25.00 ©2010 IEEE

contact pads on the device. Figure 2 shows the fabricated MEMS antenna platform capable of rotation around the two sets of torsion hinges.

Fig. 2. Picture of finalized MEMS antennas with SMA connectors

Antenna Measurements

The antenna performance is measured using the HP 8510C Vector Network Analyzer (VNA) and the measurements are performed in a custom built 1m×1m×1m anechoic chamber. The VNA is calibrated using the 85052C 3.5mm precision calibration kit to ensure the measurement plane is at the end of the cables. The scattering parameters of the antennas are measured and shown in Fig. 3. The simulated results shown in Fig. 3 are obtained using the Ansoft High Frequency Structure Simulator (HFSS).

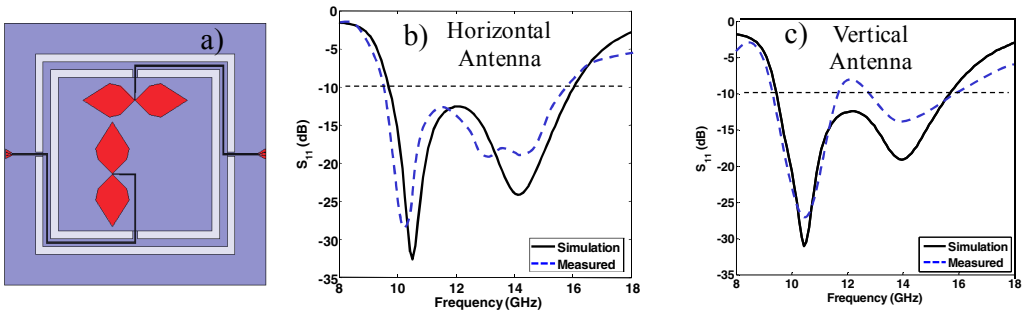

Fig. 3. a) The geometry simulated in HFSS along with the measured and simulated S_{11} for the b) horizontal antenna and c) vertical antenna

The results of Fig. 3 show reasonable agreement between the measured and simulated S_{11}. The horizontal antenna remains well matched within the 10-16GHz band as shown in Fig. 3b. The S_{11} for the vertical antenna rises above -10dB at 12GHz as shown in Fig. 3c. The loss of matching for the vertical antenna is partially attributed to the additional corner present in the CPW feedline. The same observations were made by Hutchings *et al.* [4]

Target Detection using Artificial Neural Networks

The open source back propagation neural network software, NevProp v1.6, was utilized for target detection. Previous, Woten *et al.* focused on the implementation of the neural network using synthetic data [5]. The network was fully interconnected with a single hidden layer. Fifty-one input nodes were used corresponding to the measured S-parameters every 100 MHz from 10.5-15.5 GHz. The hidden layer was composed of nine

hidden nodes and the output layer contained a single node which output a number between 0 and 1.

The target objects were spherical with a diameter of 3/8″. Three example object types are investigated; metal, glass and wood with permittivity of 5.5 for the glass and 3.7 for the wood. These three materials were chosen for their dielectric properties which provided a large range of electromagnetic scattering. The backscatter and forward scatter configurations were investigated for each of the target objects.

In the first case, the backscatter data was used as the input for the neural network. The backscatter data was measured by the S_{11} of the antenna shown in Fig. 2. A total of two-hundred measurements were collected with one-hundred cases having the target object present and one-hundred cases having no target present. The target was relocated slightly between each measurement and rotated to ensure measurement data was not completely identical. Half of the cases (fifty with the object and fifty without) were used to train the neural network and the remaining cases were used as the testing set. The number of cases that are correctly identified by the network and the number of false predictions are recorded. The neural network results for the backscattered measurements are shown in Fig. 4a.

A Receiver Operating Characteristic (ROC) Curve is a graphical representation of the tradeoff between the false negative and false positive rates for every possible cutoff as shown in Fig. 4b. Typically the probability of detection (1- false negative rate) is plotted on the vertical axis and the false positive rate is plotted on the horizontal axis. The larger the area under the ROC curve the better the diagnostic test and a satisfactory test should climb rapidly towards a value of 1 on the vertical axis [6]. The optimum cutoff (which depends on the severity of false positives and false negatives) can be found through a systematic analysis of the ROC curve.

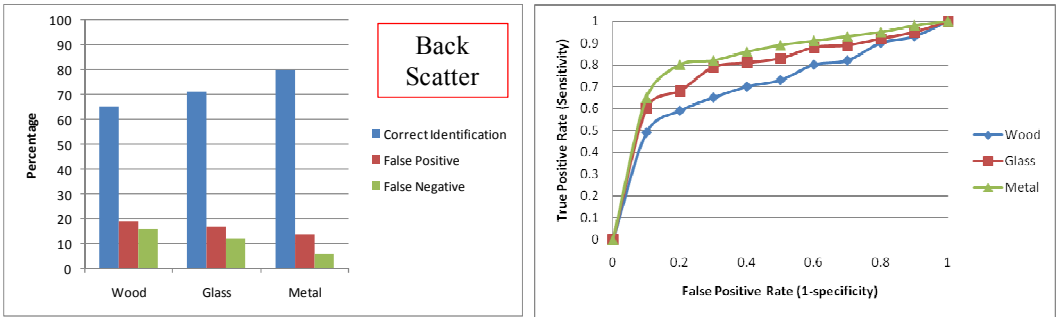

Fig. 4. a) Artificial neural network results for backscattered data for each of the target types and b) the ROC curve for the backscattered data

The number of correct identifications in Fig. 4 increases with the strength of the scattering object. Metal is a very strong scatterer of electromagnetic fields and the network made the most correct identifications with the metal object. Wood, on the other hand, is the weakest of the scattering objects and the network made more incorrect predictions with the wooden sphere. It is interesting to note that the number of false positive results differ very slightly between the object types while the number of false negatives accounted for the majority of the decrease in detection.

The forward scattered data was collected with the same configuration as the backscatter data, except with a second antenna placed on the opposite side of the object. The neural network results are shown in Fig. 5a and the corresponding ROC curve is shown in Fig. 5b. The results of Fig. 5 show that the number of correct identifications is highest for the metal target and lowest for the wood target. This is consistent with the results for the backscattered data shown in Fig. 4.

Fig. 5. a) Artificial neural network results for forward scattered data for each of the target types and b) the ROC curve for the forward scattered data

In this work, the ANN achieved a higher correct identification percentage for each of the three objects when using the forward scattered data. In Fig. 4 it was the number of false negative results that increased as the scattering object became weaker, while in Fig. 5 it is the false positive results that increase predominately.

Acknowledgements

This work was supported in part by the NSF Graduate Research Fellowship, National Science Foundation GK-12 Program and the High Density Electronics Preliminary Research Proposal (PReP) Program.

References

[1] S. Lee, J.M. Kim, J.M. Kim, Y.K. Kim, C. Cheon, Y. Kwon, "V-band Single-Platform Beam Steering Transmitters Using Micromachining Technology," Proc. IEEE MTT-S Microwave Symposium, 11-16 June 2006, pp. 148-151.

[2] D. Hutchings, "Design, Fabrication and Testing of Broadband MEMS Antennas," PhD Dissertation, University of Arkansas, Fayetteville, AR, USA, 2010.

[3] Seong-Youp Suh, "A Comprehensive Investigation of New Planar Wideband Antennas," PhD Dissertation, Virginia Polytechnic Institute, Blacksburg, VA, USA, 2002.

[4] D. Hutchings, M. El-Shenawee and S. Tung, "Design and Fabrication of a MEMS Steerable Broadband Antenna Capable of Dual Polarization," *Proc. of the 2010 USNC-URSI National Radio Science Meeting*, Boulder, Colorado, Jan. 6-9, 2010.

[5] D. A. Woten and M. El-Shenawee, "Broadband Dual Linear Polarized Antenna for Statistical Detection of Breast Cancer," *IEEE Trans Antennas and Propagation*, Vol. 56, no. 11, pp. 3576-3580, Nov. 2008.

[6] D. A. Woten, J. Lusth and M. El-Shenawee, "Interpreting Artificial Neural Networks for Microwave Detection of Breast Cancer," *IEEE Microwave and Wireless Components Letters*, Vol. 17, no. 12, pp. 825-827, Dec 2007.